Charge Parametrization of the DvH-c(3) Heme Group: Validation Using Constant-(pH,E) Molecular Dynamics Simulations

ARTICLE *in* THE JOURNAL OF PHYSICAL CHEMISTRY B · NOVEMBER 2012

Impact Factor: 3.3 · DOI: 10.1021/jp3082134 · Source: PubMed

4 AUTHORS, INCLUDING:

João Henriques
Lund University
7 PUBLICATIONS **23** CITATIONS
SEE PROFILE

Paulo Jorge Costa
University of Aveiro
63 PUBLICATIONS **1,151** CITATIONS
SEE PROFILE

Miguel Machuqueiro
University of Lisbon
36 PUBLICATIONS **704** CITATIONS
SEE PROFILE

THE JOURNAL OF PHYSICAL CHEMISTRY B

Article

pubs.acs.org/JPCB

Charge Parametrization of the DvH-c_3 Heme Group: Validation Using Constant-(pH,*E*) Molecular Dynamics Simulations

João Henriques,[†] Paulo J. Costa,[‡] Maria José Calhorda,[†] and Miguel Machuqueiro*[,†]

[†]Centro de Química e Bioquímica and Departamento de Química e Bioquímica, Faculdade de Ciências, Universidade de Lisboa, 1749-016 Lisboa, Portugal

[‡]Departamento de Química, CICECO and Secção Autónoma de Ciências da Saúde, Universidade de Aveiro, 3810-193 Aveiro, Portugal

Supporting Information

ABSTRACT: We studied the effect of using different heme group charge parametrization methods and schemes (Merz−Kollman, CHELPG, and single- and multiconformational RESP) on the quality of the results produced by the constant-(pH,*E*) MD method, applied to the redox titration of *Desulfovibrio vulgaris* Hildenborough cytochrome c_3. These new and more accurate charge sets enabled us to overcome the previously reported dependence of the method's performance on the dielectric constant, ε, assigned to the protein region. In particular, we found a systematic, clear shift of the E^{mod} toward more negative values than those previously reported, in agreement with an electrostatics based reasoning. The simulations showed strong coupling between protonating/redox sites. We were also able to capture significant direct and, especially, indirect interactions between hemes, such as those mediated by histidine 67. Our results highlight the importance of having a good quantum description of the system before deriving atomic partial charges for classic force fields.

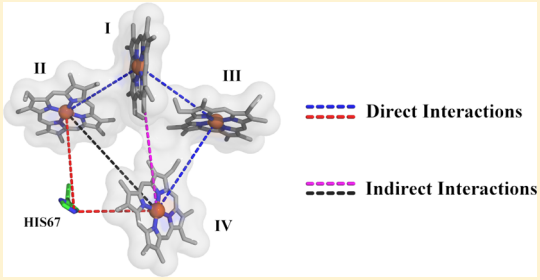

INTRODUCTION

The coupling of redox processes with protonation events is known to be essential for living organisms, playing a crucial role in respiration, photosynthesis, and other energy transduction systems. This type of interaction was named as the redox-Bohr effect.[1] It can be described as a strong pH influence on heme reduction potentials, corresponding to a thermodynamic dependence between the reduction of redox sites and the ionization of protonable sites, due to their electrostatic interaction. This effect is of potential physiological significance in cytochromes c_3, since it occurs even at physiological pH values. Therefore, the redox-Bohr effect is thought to allow (thermodynamically) correlated electron and proton capture in the same molecule, which constitutes a physiologically relevant mechanism of transferring the electrons and protons generated by hydrogenase from molecular hydrogen oxidation. While hemes receive the generated electrons, protonatable sites in the protein are more susceptible to be protonated by consequent shifts in their pK_a values.[2−9]

Throughout the years a great effort has been put toward understanding the molecular basis, regulation, and structure−function relationship of protein electron transfer. Even though this has been very well characterized experimentally (mainly thermodynamically) in tetraheme cytochromes c_3,[2−5,8] many researchers have turned to computational methods in order to understand its molecular basis and, in particular, to identify key events in the process.[10−16] With electrostatic interactions being a key factor behind the thermodynamics of a redox center, it is not surprising that earlier studies mainly focused on continuum electrostatics methods (e.g., Poisson−Boltzmann, PB) coupled with Monte Carlo (MC) sampling of the protonation/reduction states.[10,12−15] Others relied on molecular mechanics/dynamics (MM/MD), where protein conformation changes are explicitly treated for a fixed ionization (driven by protonation or reduction).[11,15]

When taken individually, PB/MC and MM/MD methods seem quite incomplete, as PB/MC methods are well adapted to describe electrostatic changes on nonflexible molecules, whereas MM/MD methods deal essentially with conformational aspects of molecular species. However, if taken together these distinct methods exhibit somewhat complementary characteristics, which were used by several authors, giving birth to a few constant-pH MD methods and subsequent extensions/implementations.[16−31] The theoretical aspects behind most constant-pH MD methods can in principle also be used to address redox processes. Recently, Machuqueiro and Baptista introduced the constant-(pH,*E*) MD method,[16] an extension to the stochastic titration method.[27] With this method it is possible to sample both the conformation and protonation/reduction states of a protein on a solution with a given pH and redox potential (E) value. The authors observed a dependence of the quality of their results on the dielectric constant, ε,

Received: August 17, 2012
Revised: November 27, 2012
Published: November 30, 2012

dx.doi.org/10.1021/jp3082134 | *J. Phys. Chem. B* 2013, 117, 70−82

assigned to the protein. This should only be expected for rigid-structure PB/MC studies, where the structural reorganization must be entirely captured by the dielectric constant. Non-structural events, such as charge redistribution upon change in heme redox state, were proposed as the main cause for the poor results at low ε.

Most current force fields use a fixed-charge model, each atom being assigned a single value for the atomic charge that is not affected by the local electrostatic environment. However, the accumulation of charge resulting from the nonuniform electronic distribution over the atoms of the system will depend not only on the type of bonds but also on its general environment, which may either exert a further increase on the asymmetry of the electronic distribution or attenuate it. The inclusion of electronic polarizability on force fields would, in principle, solve this problem, making them much less system-dependent. Yet, the introduction of polarizability into available force fields has been inhibited by the high computational expense associated with calculating the local electrostatic field. Therefore, accurate determination of the characteristic partial atomic charges of a given system is crucial for the performance of the force field used in MM/MD.[32]

There are essentially two routes for determining the parameters of the potential energy function, either fitting them to the results of ab initio quantum calculations or to experimental data. Most force fields include parameters generated with both approaches, rendering them semiempirical. Despite this, and regardless of the parametrization protocol policy behind each force field, partial atomic charges are, for practical reasons, mainly obtained from quantum mechanical computations. However, there is no universally accepted procedure, as the concept of partial atomic charge remains nonconsensual.[33] Partial atomic charges, unlike the electron density, are not a quantum mechanical observable; that is, they can not be calculated from first principles. Hence, all charge derivation methods are ultimately arbitrary. They can, however, be compared on the basis of the electrostatic performance of their partial atomic charges for a given molecular system.

GROMOS force field charge parameters may be determined from different levels of quantum theory and basis sets, as long as they are well supported and lead to a good electrostatic representation of the system.[34,35] Machuqueiro and Baptista[16] adopted Oliveira et al.[36] partial atomic charges for the redox centers, but this charge set was unable to cope with the significant charge redistribution resulting from high heme−heme interactions at low ε.[16] A possible problem may lie in the fact that it was derived from the computed molecular electrostatic potential (ESP) of the X-ray structure of only one of the four hemes (heme I) present in *Dv*H-c_3. Also, owing to the structural nature of the heme group, some atoms (i.e., Fe) are buried deep inside the molecular surface and their point charges can be wrongly determined, resulting in conformation dependent charge sets.

In order to overcome these limitations, the electronic detail of the system can be increased by performing full or partial geometry optimizations at a given QM level of theory for each heme structure at both redox states. Crystallographic X-ray structures are available for specific redox states, and hemes undergo redox-dependent conformation changes. Finally, considerable attention should also be given to the different charge derivation methods, especially to the ones which allow a multiconformational analysis.

The most commonly used methods for deriving partial atomic charges from quantum mechanically computed molecular electrostatic potentials are Merz−Kollman (MK),[37,38] CHELPG (charges from electrostatic potentials using a grid based method),[39] and RESP (restrained electrostatic potential) fitting.[40]

In both MK and CHELPG methods, partial atomic charges are fitted to reproduce the molecular ESP at a number of points around the molecule. The ESP is one of the most obvious properties to reproduce in order to get proper partial atomic charges to model short to long-range molecule−molecule interactions.[33,40,41] Those two methods mainly differ in the choice of the points where the electrostatic potential is calculated. ESP based methods are usually less sensitive to the level of theory and basis sets used in the quantum calculations than methods based on an analysis of the wave function. The obtained charges are much more dependent on the conformation of the molecule. The representative partial atomic charges for flexible molecules should hence be computed as average values over several molecular conformations.[40−42] Furthermore, one needs to be aware that buried atoms, located far away from the points at which the ESP is computed, may yield fuzzy results.

The RESP method was developed to tackle the aforementioned problems with the MK and CHELPG methods. This is done by including a penalty function in the least-squares charge fitting procedure, in the form of restraints on non-hydrogen atomic charges to a target charge. The objective of the restraints is to hold down the ESP derived charges to a lower magnitude with only a minimal decrease in the quality of the fit.[40] Apart from the possibility of restraining partial atomic charges to a certain value, the RESP fitting process allows the use of forced symmetry and multiconformational ESP derived charge fitting. Unrestrained ESP derived charges (MK) and the charges obtained from the population analysis methods, e.g., Mulliken charges,[43] perform poorly when compared with RESP derived charges, for the simulation of biomolecules.[44] Taking into account the work by Oliveira et al.,[36] and for comparison purposes, we also decided to explore all three methods directly over the X-ray structures of reduced and oxidized heme I of *Dv*H-c_3.

Desulfovibrio vulgaris Hildenborough cytochrome c_3 is a small (M_r 13,000) globular and monomeric tetraheme protein present in the periplasm of the sulfate reducing bacteria *D. vulgaris* Hildenborough, consisting of 107 residues plus four hemes covalently bound to cysteines in the polypeptide chain, together with bis-histidinyl axial ligation.[45] *Dv*H-c_3 plays an important role in the periplasmatic metabolism of molecular hydrogen in sulfate-reducing bacteria, acting as a mediator between the periplasmatic hydrogenase (the electron donor) and the high molecular weight cytochrome (the electron acceptor).[45,46] *Dv*H-c_3 hemes are covalently held together in close proximity, exhibiting strong coupling between themselves and nearby acid/base groups. The heme reduction potential is thus dependent on the oxidation state of the other three hemes (redox interaction potential) and on the pH (redox-Bohr effect). Together with a very low residue to heme ratio, we obtain a tight packed structure where the heme reduction potentials are very close (within a range of 80 mV or 1.3 pH units). This makes *Dv*H-c_3 an extremely demanding test case for reduction potential prediction, considering that 1.3 pH units is close to the constant-pH MD method pK_a prediction error reported previously.[30]

dx.doi.org/10.1021/jp3082134 | J. Phys. Chem. B 2013, 117, 70−82

COMPUTATIONAL DETAILS AND METHODS

Parametrization of the Redox Centers. All quantum mechanical calculations were performed with the program Gaussian 03,[47] using the B3LYP functional and LANL2TZ(f) or 6-31G(d) basis sets for Fe and all other atoms, respectively.[48−54] The effective core potential LANL2TZ(f) was used for d^6 and d^5 iron atoms. All charge parametrizations were performed on *Dv*H-c_3 heme(s) I or I−IV, depending on the nature of the charge derivation scheme, i.e., single- or multiconformational. *Dv*H-c_3 heme models (see Figure 1)

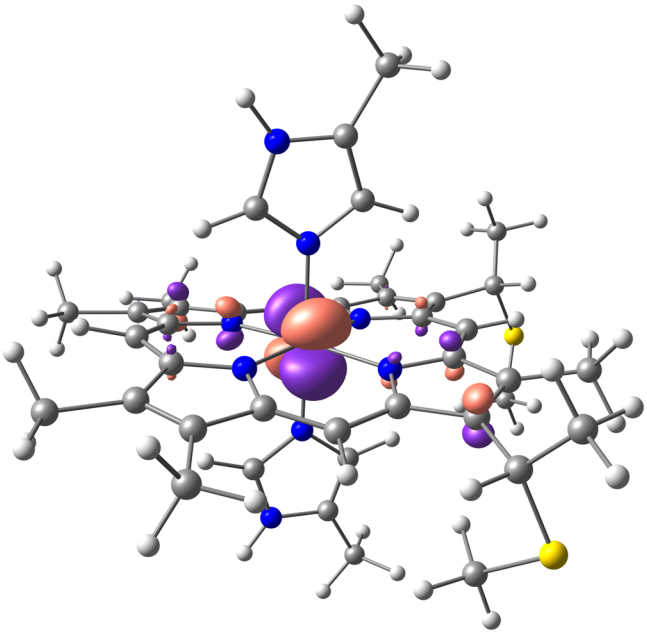

Figure 1. HOMO representation of the reduced d^6 Fe(II) in heme I X-ray model. Orbitals were rendered using Chemcraft.[71]

consisted of the respective heme c group, the axial histidines side chains and covalently bound cysteine side chains of molecule A of the X-ray structure of this cytochrome (Protein Data Bank entry 2CTH).[55,56] 2CTH has two molecules in the asymmetric unit with almost identical conformations; therefore, we only used one in this study. Both histidine and cysteine side chains are separated from the rest of the respective amino acid at the C_β, which is treated as a methyl group in the model. Heme propionates were treated as independent titrating sites and, therefore, were not included in the heme model structure for charge parametrization. Each heme group is similar in chemical formulation, differing uniquely in its (X-ray) conformation. The open source chemistry toolbox OpenBabel was used to automatically introduce all hydrogens in each model.[57] Since cytochrome c_3 heme-iron is low spin in both Fe(II) and Fe(III) states, all systems were treated as having a spin multiplicity of 1 and 2, respectively,[58,59] corresponding to an overall charge of 0 and 1.

Six different charge derivation schemes were performed. CHELPG, MK, and single-conformational RESP fitting procedures were performed over *Dv*H-c_3 heme I X-ray structure model without geometry optimization. A multiconformational RESP fitting was also performed over the models of *Dv*H-c_3 hemes I−IV using the unrelaxed X-ray structures (RESP MC X-ray). Finally, the two remaining charge sets were computed with a multiconformational RESP calculation on the DFT geometry-optimized models of *Dv*H-c_3 hemes I−IV (RESP MC Free Opt) or optimized with constraints on critical atoms, i.e., the axial histidine and covalent cysteine C_β atoms (RESP MC Fixed Opt). With this last charge set, we aim to model the expected heme group nonplanarity by freezing the atom positions identified as its key determinants.[60] Each geometry optimization was followed by a frequency calculation to ensure that all optimized geometries represented a local/global minimum of the respective potential energy landscape.

The RESP fitting procedure was done using a modified version of the AmberTools 1.3 RESP program, i.e., a patched standalone version of the RESP program obtained from http://q4md-forcefieldtools.org.[61,62] The patched version was chosen since the standard RESP program handles only a limited number of ESP points, which proved to be insufficient for the desired level of accuracy.

All charges related to the apolar hydrogen atoms which are omitted in the united-atom MD heme group model were summed into their covalent heavy atom partial charge. Notice that in GROMOS 53A6 the united-atom model of the histidine residue side chain comprises two more hydrogen atoms than that from GROMOS 43A1.[34,35] This results in four more heme group charged atoms for the GROMOS 53A6 force field.

Redox Titrations. All MM/MD and PB/MC simulations of *Dv*H-c_3 were performed using the constant-(pH,*E*) MD method.[16] The six, previously mentioned, heme charge parametrizations were included in the original GROMOS 53A6 force field. An appropriate RESP X-ray parametrization was also added to the GROMOS 43A1 force field (the number of hydrogen atoms is different between 43A1 and G53A6), for a force field effect study. Fourteen protonable/reducible sites, including hemes I−IV, their respective propionates A and D, histidine 67, and the N-terminal were titrated at the pH value of 6.6 and reduction potentials of −140, −180, −220, −240, −260, −280, −300, and −320 mV.

Each solvent relaxation and full MM/MD cycles were 0.2 and 2 ps long, respectively. All conditions were simulated with three replicates, 15 ns each. A total of 144 (53A6) plus 24 (43A1) simulations, 15 ns long each, were performed, yielding a total ∼2.5 μs of simulation.

The heme redox titrations were computed by averaging at each redox potential the occupancy states of all four sites over the final equilibrated segment, i.e., the last 10 ns of each run. The data for each heme was fit to a Hill equation in accordance with Machuqueiro and Baptista.[16]

MEAD 2.2.0 and PETIT 1.5 were used for PB and MC calculations, respectively.[12,63] PB atomic charges and radii were taken from each modified GROMOS force field. Dielectric constants of 2 and 80 were used for protein and solvent, respectively. Temperature and ionic strength were set to 300 K and 0.1 mol/dm^3, respectively. The PB equation was solved using the finite difference procedure with grid spacings of 0.25 and 1.0 Å. Each MC calculation was performed with 10^5 iterations.

MM/MD simulations were performed using a modified version of GROMACS 3.2.1.[64,65] *Dv*H-c_3 was placed in the center of a rhombic dodecahedric box with periodic boundary conditions, filled with 5879 water molecules from a simple point charge (SPC) water model.[66] The minimum distance between images of *Dv*H-c_3 was always higher than 20 Å. The equations of motion were integrated with a 2 fs time interval and bond constraining was achieved by applying the LINCS algorithm.[67] Nonbonded interactions were treated using a twin-

dx.doi.org/10.1021/jp3082134 | J. Phys. Chem. B 2013, 117, 70−82

range cutoff scheme with values of 8 and 14 Å. The neighbor list was updated every 5 integration time steps or, in other words, every 10 fs. Long range electrostatic interactions were treated with the generalized reaction field method, in which a dielectric constant of 54 was used.[68] The ionic strength was set at 0.1 mol/dm^3. Pressure and temperature were kept constant during the course of each simulation through the use of Berendsen's weak coupling methods.[69] Berendsen's thermostat was set to yield a constant bath temperature of 300 K with a coupling constant, τ, of 0.1 ps. Pressure was kept constant at 1 bar, while the coupling constant was set to 2 ps. Isothermal compressibility was set to 4.5×10^{-5} bar^{-1}.

Before each MM/MD simulation, an energy minimization of each system (fully reduced and fully oxidized) was performed. All bonds were constrained by LINCS. Different MM/MD initiations were done for each *Dv*H-c_3 heme redox state, charge set, and respective replicate. The first initiation was 50 ps long and all protein atoms were restrained (1000 kJ mol^{-1} nm^{-1}). Velocities were generated with different seeds for each of the three replicates. In the second initiation only C_α were restrained.

All analyses were performed using the GROMACS package and in-house tools. Structural representations were done using PyMOL 0.99rc6[70] and Chemcraft 1.6,[71] while graphics were generated using Gnuplot 4.2 patchlevel 4.[72] The calculations of correlation-corrected errors for averages were computed using standard methods based on the autocorrelation function of the property measured to determine the number of independent blocks in the simulations.[73]

RESULTS AND DISCUSSION

Charge Determination: Electronic Population. An electronic population analysis of all QM calculations for charge set derivation was conducted. As can be seen in Figure 1, in reduced systems the HOMO is a t_{2g} orbital localized on the iron atom and, upon oxidation, the spin density was found mainly over the hemic iron atom (1.071). No significant spin contamination was found in any tested oxidized heme model. Spin contamination is negligible if the value of $\langle S^2 \rangle$ differs from $s(s + 1)$ by less than 10%.[33] These results indicate that the B3LYP functional, with the used basis set is appropriate to describe the ground state electronic structure of the heme model.

Charge Determination: Geometry Optimization. The heme group charges used by Machuqueiro and Baptista in the implementation of the constant-(pH,*E*) MD method were those previously published by Oliveira et al. in 2005.[16,36] The charges were obtained by a RESP fitting procedure of the electrostatic potential from the X-ray structure of *Dv*H-c_3 heme number one (for short: heme I X-ray). The buried Fe charges were left unrestrained, which may lead to poor predictions. These charges were applied to all four heme groups without taking into account that each heme group has its own unique conformation. Furthermore, each heme undergoes a conformational change upon oxidation, which leads to eight different heme conformations. Also, because the X-ray heme group conformation is not necessarily the same as in solution, geometry optimizations can be used to relax the structures and eliminate intramolecular crystal strain. In this case, we performed two different approaches: a free optimization (no positional freezing) and a fixed optimization, where the axial histidines and covalent cysteines C_β atoms were fixed to their X-ray position.

Table 1 shows the RMSD values between hemes before and after geometry optimizations. It is clear that heme III presents

Table 1. Structure RMSD Crossing Table[a]

				I X-ray	II X-ray	III X-ray	IV X-ray
heme	I	X-ray		0			
		fixed	reduced	0.228			
			oxidized	0.212			
		free	reduced	0.320			
			oxidized	0.332			
	II	X-ray		0.386	0		
		fixed	reduced	0.441	0.221		
			oxidized	0.443	0.232		
		free	reduced	0.467	0.321		
			oxidized	0.503	0.331		
	III	X-ray		0.670		0	
		fixed	reduced	0.719		0.241	
			oxidized	0.710		0.240	
		free	reduced	0.750		0.277	
			oxidized	0.746		0.266	
	IV	X-ray		0.486			0
		fixed	reduced	0.320			0.321
			oxidized	0.370			0.317
		Free	reduced	0.333			0.448
			oxidized	0.370			0.457

[a]Optimized heme structures against heme X-ray (Å).

the conformation most different from heme I X-ray (0.67 Å). Even though hemes I and II appear to be relatively close (0.39 Å), assigning the same charge set to all hemes regardless of their conformational differences can indeed be a significant approximation, especially when these charges are derived from a single X-ray structure, which is by no means representative of any heme group present in a protein in solution, at any given redox state. Thus, we need to use a less conformationally dependent charge derivation method, as CHELPG, or a multiconformational approach, like RESP.

All optimized structures were also compared to the X-ray structure of heme I, primarily showing how much each heme group deviates from its original X-ray structure upon geometry optimization. It also shows how different each heme group is from the heme I X-ray structure, used primarily by Oliveira et al. in their heme group charge parametrization.[36] In general terms, all optimized heme groups seem to deviate in the same proportion from their original X-ray structure. Heme IV is the outlier here, as it relaxes significantly more than the others. The redox state seems to influence structure optimization, but to a lesser extent. Full and partial optimizations, even when only 4 atoms out of 99 are restricted to their X-ray positions, constitute indeed two different approaches, with markedly different RMSD values.

Charge Determination Analysis. Table 2 comprises all of the partial atomic charges obtained for each charge set. The charges of apolar hydrogens were added to their respective heavy atoms charge, according to the heme group model present in united-atom force fields.

Certain empirical rules should be followed by the different charge groups. For example, the partial atomic charges of the heme-iron atom (ferrous and ferric) should be positive, whereas nitrogen atoms will probably have a negative partial atomic charge. Furthermore, oxidized iron should in principle present

dx.doi.org/10.1021/jp3082134 | J. Phys. Chem. B 2013, 117, 70−82

Table 2. Atomic Partial Charge for the Six Different Charge Sets[a]

		CHELPG		MK		RESP		RESP MC X-ray		RESP MC fixed opt		RESP MC free opt	
	atom	reduced	oxidized	reduced	oxidized	reduced	oxidized	reduced	oxidized	reduced	oxidized	reduced	oxidized
1	FE	0.958	1.152	0.674	0.663	0.491	0.686	0.477	0.666	0.480	0.666	0.478	0.676
2	NA	−0.469	−0.488	−0.366	−0.360	−0.331	−0.355	−0.198	−0.215	−0.134	−0.153	−0.094	−0.144
3	NB	−0.235	−0.279	−0.124	−0.176	−0.137	−0.221	−0.209	−0.291	−0.249	−0.256	−0.187	−0.286
4	NC	−0.320	−0.343	−0.240	−0.252	−0.168	−0.231	−0.248	−0.310	−0.198	−0.239	−0.151	−0.235
5	ND	−0.498	−0.533	−0.338	−0.344	−0.351	−0.379	−0.266	−0.218	−0.102	−0.113	−0.117	−0.159
6	CHA	−0.258	−0.265	−0.026	−0.061	−0.032	−0.071	−0.059	−0.041	0.018	−0.004	0.030	0.017
7	HHA	0.159	0.171	0.124	0.145	0.117	0.139	0.101	0.117	0.095	0.109	0.092	0.105
8	C1A	0.186	0.206	−0.138	−0.091	−0.122	−0.073	−0.073	−0.059	−0.155	−0.110	−0.178	−0.138
9	C2A	−0.064	−0.041	0.173	0.172	0.174	0.169	0.116	0.112	0.119	0.113	0.120	0.127
10	C3A	0.002	0.015	0.100	0.095	0.088	0.091	0.131	0.139	0.123	0.148	0.131	0.136
11	C4A	0.160	0.186	0.030	0.085	0.029	0.077	−0.097	−0.046	−0.096	−0.091	−0.133	−0.076
12	CMA	−0.010	0.029	−0.085	−0.037	−0.080	−0.034	−0.083	−0.039	−0.072	−0.037	−0.073	−0.035
13	CAA	−0.012	0.025	−0.097	−0.050	−0.094	−0.047	−0.083	−0.038	−0.069	−0.028	−0.068	−0.030
14	CHB	−0.231	−0.233	−0.117	−0.154	−0.112	−0.145	−0.039	−0.069	−0.091	−0.073	−0.056	−0.088
15	HHB	0.147	0.158	0.135	0.154	0.135	0.152	0.126	0.138	0.122	0.130	0.117	0.134
16	C1B	0.042	0.083	−0.109	−0.012	−0.068	0.013	−0.130	−0.062	−0.052	−0.035	−0.109	−0.011
17	C2B	0.015	0.006	0.159	0.103	0.110	0.077	0.186	0.175	0.151	0.125	0.175	0.122
18	C3B	−0.109	−0.047	0.110	0.186	0.177	0.218	0.080	0.091	−0.012	0.059	−0.004	0.070
19	C4B	0.139	0.151	−0.151	−0.119	−0.181	−0.117	−0.067	0.046	0.031	0.036	−0.025	0.034
20	CMB	−0.016	0.023	−0.080	−0.029	−0.072	−0.025	−0.088	−0.046	−0.067	−0.025	−0.070	−0.026
21	CAB	0.442	0.384	0.222	0.159	0.174	0.123	0.147	0.105	0.133	0.083	0.133	0.073
22	CBB	−0.114	−0.080	−0.080	−0.046	−0.068	−0.035	−0.050	−0.022	−0.021	0.009	−0.024	0.010
23	CHC	−0.330	−0.308	−0.246	−0.236	−0.208	−0.214	−0.159	−0.252	−0.182	−0.195	−0.126	−0.155
24	HHC	0.186	0.183	0.189	0.188	0.171	0.173	0.138	0.180	0.132	0.143	0.132	0.136
25	C1C	0.182	0.202	−0.022	0.027	−0.037	0.023	−0.051	0.078	−0.062	0.022	−0.142	−0.025
26	C2C	−0.011	−0.021	0.207	0.166	0.173	0.133	0.222	0.149	0.203	0.164	0.253	0.205
27	C3C	−0.192	−0.119	−0.157	−0.086	−0.104	−0.030	−0.110	−0.063	−0.045	−0.006	−0.051	−0.014
28	C4C	0.167	0.171	0.064	0.097	0.013	0.052	0.049	0.062	−0.037	−0.041	−0.037	−0.006
29	CMC	−0.017	0.026	−0.074	−0.021	−0.064	−0.013	−0.082	−0.033	−0.077	−0.042	−0.095	−0.059
30	CAC	0.458	0.398	0.279	0.222	0.253	0.195	0.252	0.253	0.172	0.156	0.164	0.148
31	CBC	−0.098	−0.063	−0.070	−0.036	−0.065	−0.032	−0.080	−0.053	−0.038	−0.002	−0.034	0.000
32	CHD	−0.371	−0.346	−0.209	−0.217	−0.213	−0.216	−0.159	−0.144	−0.090	−0.072	−0.101	−0.110
33	HHD	0.243	0.239	0.203	0.207	0.200	0.203	0.140	0.141	0.129	0.136	0.129	0.136
34	C1D	0.218	0.240	−0.005	0.054	0.076	0.110	−0.011	−0.022	−0.137	−0.130	−0.134	−0.083
35	C2D	−0.063	−0.047	0.104	0.088	0.038	0.042	0.108	0.118	0.124	0.146	0.135	0.131
36	C3D	−0.023	−0.003	0.137	0.147	0.197	0.190	0.097	0.117	0.132	0.130	0.117	0.128
37	C4D	0.213	0.235	−0.116	−0.078	−0.155	−0.099	−0.016	−0.048	−0.167	−0.127	−0.154	−0.115
38	CMD	−0.015	0.021	−0.087	−0.040	−0.078	−0.034	−0.080	−0.035	−0.068	−0.032	−0.071	−0.027
39	CAD	−0.019	0.019	−0.092	−0.046	−0.098	−0.050	−0.079	−0.037	−0.075	−0.034	−0.072	−0.032
40	CBS1	0.138	0.131	0.086	0.079	0.087	0.082	0.075	0.070	0.068	0.060	0.071	0.063
41	SGS1	−0.414	−0.350	−0.293	−0.228	−0.275	−0.212	−0.244	−0.187	−0.225	−0.157	−0.232	−0.160
42	CBS2	0.133	0.119	0.098	0.085	0.096	0.083	0.078	0.082	0.065	0.070	0.062	0.074
43	SGS2	−0.415	−0.346	−0.296	−0.229	−0.282	−0.214	−0.258	−0.222	−0.238	−0.195	−0.233	−0.195
44	CB01	−0.015	0.022	−0.084	−0.040	−0.068	−0.024	−0.048	−0.001	−0.032	0.012	−0.035	0.007
45	CG01	0.268	0.282	0.434	0.423	0.373	0.362	0.224	0.229	0.203	0.199	0.212	0.209
46	ND11	−0.467	−0.440	−0.481	−0.445	−0.428	−0.393	−0.349	−0.328	−0.345	−0.293	−0.363	−0.318
47	HD11	0.363	0.377	0.373	0.387	0.361	0.374	0.356	0.373	0.355	0.365	0.358	0.370
48	CD21	−0.116	−0.115	−0.449	−0.441	−0.429	−0.399	−0.224	−0.216	−0.217	−0.202	−0.204	−0.195
49	HD21	0.077	0.087	0.232	0.239	0.236	0.236	0.191	0.192	0.175	0.179	0.172	0.175
50	CE11	0.305	0.306	0.102	0.083	0.018	0.021	0.010	0.029	0.011	0.012	0.044	0.040
51	HE11	0.017	0.033	0.125	0.146	0.168	0.178	0.110	0.114	0.109	0.118	0.100	0.109
52	NE21	−0.424	−0.427	−0.015	0.042	0.069	0.055	−0.020	−0.031	−0.027	−0.040	−0.067	−0.053
53	CB02	−0.004	0.032	−0.063	−0.020	−0.072	−0.028	−0.052	−0.010	−0.034	0.004	−0.037	0.003
54	CG02	0.227	0.243	0.344	0.333	0.373	0.362	0.224	0.229	0.203	0.199	0.212	0.209
55	ND12	−0.427	−0.407	−0.401	−0.371	−0.428	−0.393	−0.349	−0.328	−0.345	−0.293	−0.363	−0.318
56	HD12	0.358	0.374	0.355	0.370	0.361	0.374	0.356	0.373	0.355	0.365	0.358	0.370
57	CD22	−0.196	−0.184	−0.440	−0.412	−0.429	−0.399	−0.224	−0.216	−0.217	−0.202	−0.204	−0.195
58	HD22	0.140	0.145	0.256	0.259	0.236	0.236	0.191	0.192	0.175	0.179	0.172	0.175
59	CE12	0.145	0.165	−0.020	−0.018	0.018	0.021	0.010	0.029	0.011	0.012	0.044	0.040

dx.doi.org/10.1021/jp3082134 | J. Phys. Chem. B 2013, 117, 70−82

Table 2. continued

		CHELPG		MK		RESP		RESP MC X-ray		RESP MC fixed opt		RESP MC free opt	
atom		reduced	oxidized	reduced	oxidized	reduced	oxidized	reduced	oxidized	reduced	oxidized	reduced	oxidized
60	HE12	0.083	0.090	0.182	0.194	0.168	0.178	0.110	0.114	0.109	0.118	0.100	0.109
61	NE22	−0.218	−0.244	0.074	0.097	0.069	0.055	−0.020	−0.031	−0.027	−0.040	−0.067	−0.053

[a]Atoms ordered by number and label. Single conformational charge sets were calculated on heme I and are represented simply by the method name (CHELPG, MK, and RESP). Multi-conformational approaches were calculated on the four hemes and are represented by the acronym MC with the respective geometry optimization method.

higher positive charge than its reduced counterpart. In the previously published charge set,[36] the reduced heme-iron charge was 48% higher than its oxidized counterpart. This big discrepancy is hard to interpret and probably had an important influence on the results.

Here, with the exception of MK charges, all iron and nitrogen partial atomic charges reflect formal oxidation states and electronegativity. MK charges for NE21 and NE22 (axial coordinating nitrogen atoms, belonging to the axial histidine residues) were sometimes found to assume positive values. MK Fe(II) and Fe(III) charges were also not in the right order, but the net difference between them was insignificant (1.1%). This was not completely unexpected because ESP based charge derivation methods usually yield weak charge estimates for deeply buried atoms. To overcome this problem, we used Mulliken iron charges for the RESP fittings. Despite their limitations, Mulliken charges still represent the best estimates of deeply buried atoms like heme-iron. Since they do not depend on the conformation, all RESP charge sets (single and multiconformational) have similar iron charges depending on the heme redox state.

In general, CHELPG charges follow expected trends. However, CHELPG showed a tendency to create bigger dipoles between atoms of opposite charge signal. From Tables S1 and S2 it is evident that CHELPG charges diverge significantly from all the other charge sets. The CHELPG scheme sampling method differs from that of MK and, ultimately, from RESP which is based on the MK scheme. Multiconformational approaches also yield different results from those given by single-conformation methods. For example, within the RESP approaches taken here, the resulting charges tend to diverge as the degrees of freedom allowed in the geometry optimizations are increased. Interestingly, the RMSD values between redox states shown in Table S3 are almost constant throughout the different charge sets. We also noted that the RESP fitting procedure altered the MK charges quite significantly.

Figure 2 and Figure S1 depict atoms with atomic charges varying the most throughout the six charge sets considered in this work. Atoms closer to the coordination center present the highest average variation. This is significant, as these atoms are closely involved in the redox event that occurs at each heme-iron coordination center.

Redox Titration. Following Machuqueiro and Baptista's approach,[16] a model of five pairwise interacting sites (4 redox + 1 protonable) were successfully fitted to the experimental data published by Turner et al.[4] More recently, Paquete et al. reanalyzed this data and published new thermodynamic parameters that do not differ qualitatively from the previous ones.[74] In order to compare our new results direcly with published results using this methodology, we used the original data[4] as a reference throughout this work.

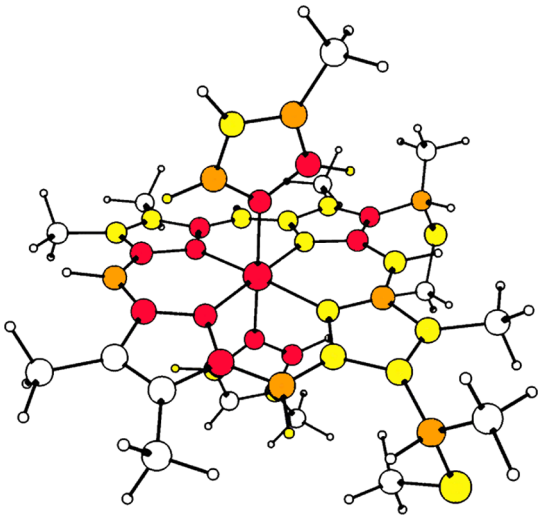

Figure 2. Color representation of the average partial atomic charge variation. Atoms with partial charge varying the most between charge sets are represented in red. From orange to white, the atomic partial charge variation decreases.

Figure 3 shows the total redox titration curves obtained using different charge sets with GROMOS 53A6 force field in

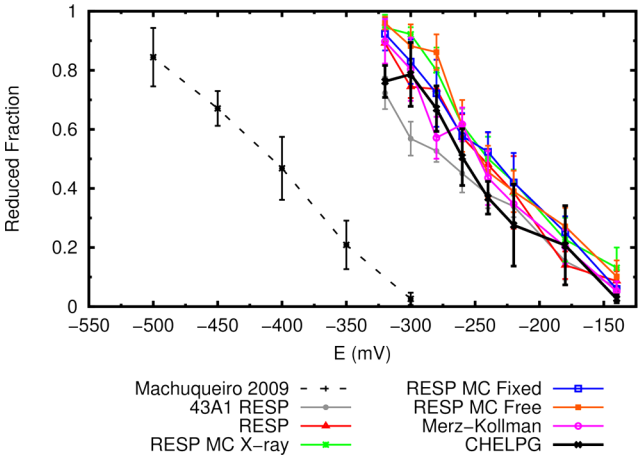

Figure 3. Redox titration curves for each charge set, using E^{mod} = −249 mV.[14] The redox titration curve corresponding to the simulations at ε = 2 from Machuqueiro and Baptista[16] is also shown in a dashed black line for comparison of results.

constant-(pH,*E*) MD simulations of *Dv*H-c_3. In order to compare with previous work,[16] we also present the redox titration curve obtained with the GROMOS 43A1 force field, using a new RESP charge set calculated on heme I X-ray (43A1 RESP). As mentioned in the Computational Details and Methods section of this work, all redox titration curves were

dx.doi.org/10.1021/jp3082134 | J. Phys. Chem. B 2013, 117, 70−82

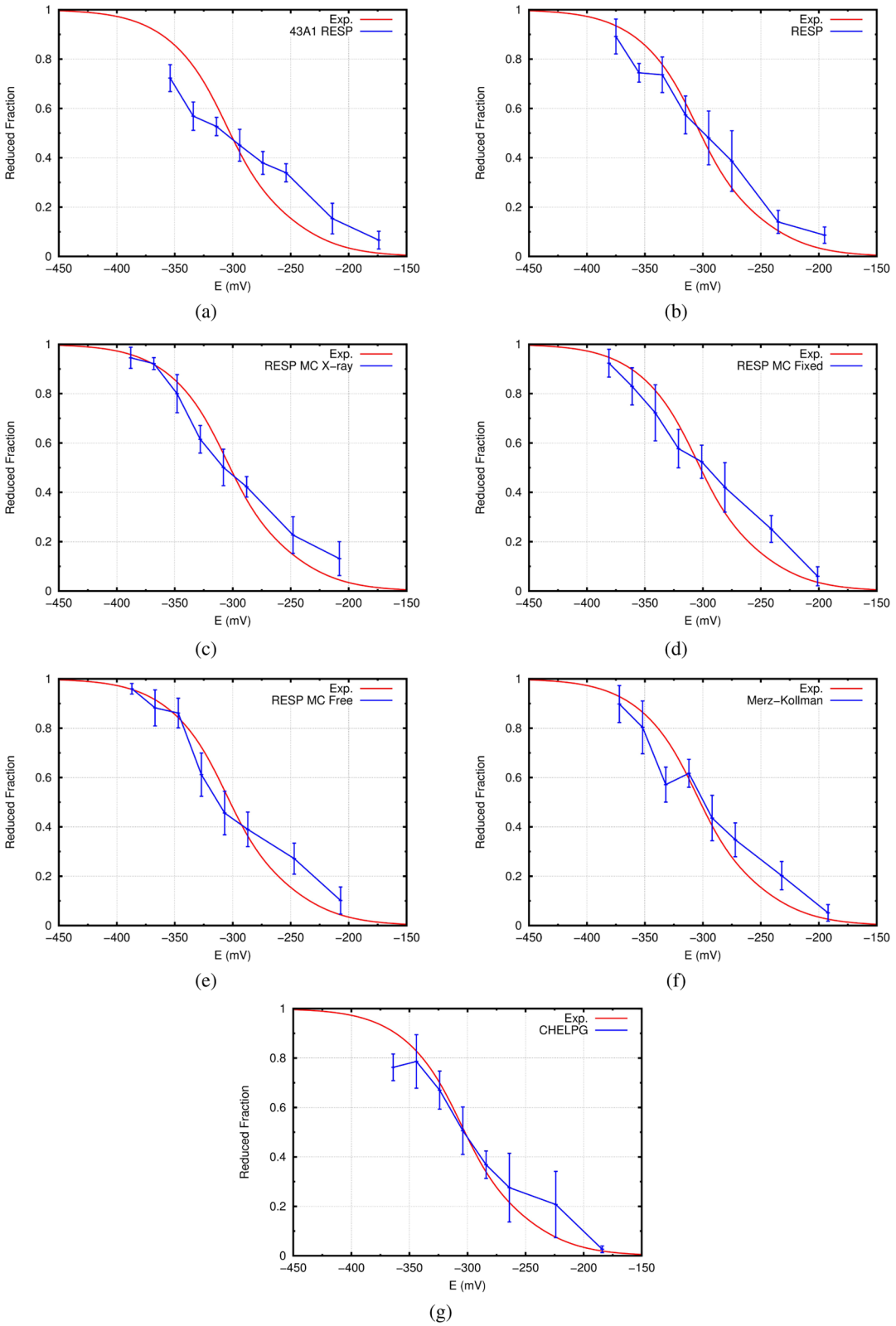

Figure 4. Total titration curves of each charge set fitted to the experimental model.[4] (a) 43A1 RESP, (b) RESP, (c) RESP MC X-ray, (d) RESP MC fixed opt., (e) RESP MC free opt. (f) MK, and (g) CHELPG.

obtained using a protein dielectric constant of 2. Once again, following a reported methodology,[16] the reduction potential of the heme model compound (E^{mod}) was taken as the value obtained in a rigid-structure PB/MC study, i.e. −249 mV.[14] The E^{mod} value corresponds to the reduction potential of a hypothetical heme model compound in solution. An experimental E^{half} (approximately −220 mV) was determined by Harbury et al. in 1965,[75] for an octapeptide bis-histidinyl derivative of the cytochrome *c* heme group. However, this heme group is affected by the particular environment and can

dx.doi.org/10.1021/jp3082134 | J. Phys. Chem. B 2013, 117, 70−82

Table 3. RMSD Values and Corresponding E^{mod} and E^{half} Obtained for Each Charge Set[a]

		E^{half} (mV)					RMSD	
charge set	E^{mod} (mV)	heme I	heme II	heme III	heme IV	range	mV	pH units
Machuqueiro and Baptista[16]	−126	−360	−316	−243	−283	117	57	0.96
43A1 RESP	−282	−252	−369	−219	−360	150	88	1.48
RESP	−304	−296	−320	−251	−334	83	58	0.98
RESP MC X-ray	−327	−303	−325	−229	−345	116	70	1.18
RESP MC fixed	−320	−312	−304	−236	−350	114	69	1.16
RESP MC free	−322	−306	−318	−242	−334	92	61	1.03
MK	−304	−306	−311	−235	−351	116	69	1.16
CHELPG	−294	−330	−297	−245	−329	85	60	1.01
experimental[4]	−220[75]	−302	−307	−336	−256	80		

[a]Experimental values are presented as a reference. Machuqueiro and Baptista's 2009 results are relative to their simulations performed at $\varepsilon = 2$. For the Hill coefficient values, see Supporting Information.

be regarded at best as an indicative value for our model compound. The Teixeira et al. rigid-structure PB/MC study showed that an E^{mod} value of −249 mV yielded the lowest RMSD between the E^{half} values obtained from experimental and theoretical methods.[14]

From Figure 3 one can clearly see the different behavior between past and present results, showing the sensitivity of the redox titration toward the different charge sets studied. Remarkably, we found a small horizontal displacement between the curves of all charge sets tested in this work. Compared to the redox titration curve extracted from Machuqueiro and Baptista,[16] our model seems to be titrating at a more plausible reduction potential range (assuming the E^{mod} value of −249 mV[14]). The proximity between our titration curves and the experimental model titration range should have a great impact on the fitted E^{mod} and E^{half} values.[4] These values, especially the E^{mod}, should agree better with each other and with experimental data, than previous published work. The charge set has a bigger or equivalent impact on the redox titration behavior than the force field used, as evidenced by comparing these results with those in the previous study using the same force field (GROMOS 43A1). Even though the partial charge derivation scheme is similar (both used a RESP fitting of the ESP of heme I X-ray structure), the quantum mechanical settings and parameters used in the computations were different. Another important difference was the use of the Mulliken partial charge for the buried iron atom. On the other hand, the redox titration curves obtained using two different force fields agree well with each other.

The redox titration curves obtained for the simulations with GROMOS 43A1 (previous and present work) present a lower slope than those simulated with GROMOS 53A6. This becomes clearer when the total titration curves are fitted to the experimental model,[4] as shown in Figure 4. This was first reported in the previous work,[16] being attributed to excessive electrostatic interactions between hemes, a consequence of the low protein dielectric constant used, $\varepsilon = 2$. With the new charge sets, the excessive electrostatic interactions seem to be attenuated and the difference in the curves between force fields can also have a noticeable contribution from the intrinsic nonbonded/electrostatic differences in GROMOS 43A1 and 53A6 force fields.[76]

Even though our results lack sampling at some regions of the titration curves, most charge sets lead to good fit to experimental data.[4] Among the GROMOS 53A6 simulations, the multiconformational RESP curves seems particularly good, the worst being relative to the CHELPG charge set.

Table 3 comprises the E^{mod} and individual heme midpoint reduction potentials (E^{half}) determined for each charge set and respective force field, and the RMSD of the computed E^{half} values relative to the experimental model. Since there is no experimental E^{mod} value for our heme model compound, we determined an optimal E^{mod} value for each charge set tested according to Machuqueiro and Baptista.[16] This was done by shifting the E values and determining the RMSD between the four computed E^{half} and those obtained experimentally, at each step. The E value which gives the lowest RMSD is taken as the best estimate of the optimal E^{mod}.

The computed E^{mod} values agree well with one another, varying smoothly around ∼−300 mV. However, they disagree greatly with the previously determined value, i.e., −126 mV.[16] A shift of the E^{mod} toward more negative values than the E^{half} obtained by Harbury et al. in their system (−220 mV)[75] is highly desirable. The reason is that our model compound heme groups are more exposed to the solvent than Harbury's octapeptide model. Considering that the oxidized form of our model has a positive global charge, it should in principle be more stable in solution than the respective octapeptide bis-histidinyl derivative counterpart. Furthermore, the propionate sites, although probably ionized at the simulated pH, are very likely to be strongly solvated, having no significant effect on the E^{mod}.[12] As a consequence, we expected the reduction potential of our model compound to be significantly more negative than the reported value, −220 mV.[12,75]

As for the E^{half} values, we noted that the values relative to each heme for each charge set are in close agreement with one another. Hemes I and II seem to titrate at relatively close reduction potentials while hemes III and IV show strong divergence in their E^{half} values. This is reflected on the heme E^{half} range. With the single exception of 43A1 RESP, the absolute E^{half} range values lie in between 83 and 116 mV. These values are in close agreement with the previously reported range for the heme reduction potential, simulated at $\varepsilon = 2$ (see Table 3 first row).[16] However, they assume marginally higher values than that reported by Turner et al. (see Table 3 last row).[4]

From the RMSD, we observed that each simulated charge set (with the exception of 43A1 RESP) yields similar results. The stochastic titration method seems to be rather robust to small changes in heme group partial atomic charge parameters. Moreover, the computed RMSD values, when translated into pH units, are close to that of the published stochastic titration method precision error, ∼0.8 pH units.[30] This emphasizes the

dx.doi.org/10.1021/jp3082134 | J. Phys. Chem. B 2013, 117, 70−82

high accuracy of the overall methodology employed in these new studies.

Table 4 presents the order of reduction of the heme groups for each charge set tested, obtained by sorting the E^{half} values of Table 3, in ascending order of E. As can be seen, previous results were not able to predict the correct order.[16] With the exception of RESP MC Fixed, CHELPG and 43A1 RESP we are able to predict correctly the relative order of reduction of heme I and II. Hemes III and IV are in the wrong order, as also happened in previous work by Machuqueiro and Baptista, even using higher dielectric constants.[16] Indeed, only when simulating at ε = 15, were the authors able to obtain the correct order of reduction for heme IV relative to heme III.

Table 4. Calculated and Experimental Order of Reduction of the Heme Groups for Each Charge Set[a]

charge set	low E	high E
Machuqueiro and Baptista[b]	I < **II** < IV < III	
43A1 RESP	II < IV < **I** < III	
RESP	IV < **II** < **I** < III	
RESP MC X-ray	IV < **II** < **I** < III	
RESP MC fixed	IV < I < II < III	
RESP MC free	IV < **II** < **I** < III	
MK	IV < **II** ≤ **I** < III	
CHELPG	I ≤ IV < II < III	
experimental[4]	**III** < **II** ≤ **I** < **IV**	

[a]Each correct heme reduction order is in boldface. [b]Machuqueiro and Baptista results are also relative to their simulations performed at ε = 2.[16]

With the exception of CHELPG and 43A1 RESP, which overestimate the negative nature of the reduction potential of hemes I and II, respectively, our results show that heme IV systematically titrated at lower E and heme III at higher E. A clear pattern can be extracted from Table 4 as E increases: IV < II ≤ I < III. The systematic nature of these results is remarkable, but, regardless of the charge set being used, calculated and experimental data are in complete disagreement when predicting the E^{half} values for hemes III and IV. Even though we are aware of the difficulty to assign the E^{half} values using NMR spectroscopy,[5] we found no ambiguity in this assignment for hemes III and IV.

Interestingly, compared to RESP, which is uniquely fitted to the X-ray structure of heme I, multiconformational charge sets do not improve greatly the quality of the results. In fact, the fitting to experimental data seems to be marginally worse, contradicting the idea that multiconformational approaches would be better suited for heme charge set determination because they comprise structural information relative to protein relaxation in solution and heme structural diversity.

Uniconformational methods like MK and CHELPG also present good fits, but CHELPG disagrees with other 53A6 simulations on the heme reduction order. On the other hand, 43A1 RESP presents the poorest fitting and the largest E^{half} range. Furthermore, the heme reduction order does not agree well with both experimental and 53A1 RESP simulations, owing to the poor estimation of the reduction potentials of hemes I and II, respectively. Yet, as mentioned before, the computed E^{mod} value seems to be a lot more reasonable than that reported by Machuqueiro and Baptista.[16]

Coupling between Sites and Electron Populations. Even though E^{mod}, E^{half}, and RMSD analyses are very informative about the quality of the theoretical predictions done in this work, they do not give enough insight about intermolecular interactions, i.e., homotropic and heterotropic events. This can be assessed by determining the coupling between titrating sites. Coupling between sites, especially electron−proton couplings, are usually analyzed in terms of direct interactions. A direct interaction can only occur between two neighbor sites which are directly influenced by each other electrostatic properties. Distant sites can only show measurable coupling effects through indirect interaction(s). An example of indirect coupling is the interaction between hemes I and IV of *Dv*H-c_3. These two heme groups are too far away from each other to influence directly their electrostatic potential. Yet, both hemes interact directly with heme III. A direct interaction between hemes I and III can result in a perturbation of the interaction between hemes III and IV. Thus, hemes I and IV are able to interact indirectly through heme III. An appropriate measure for coupling is the calculation of the statistical correlation between the binding states for a given pair of sites. Therefore, we present the computed correlations between all possible nonredundant pairs of titratable sites (i,j) as a function of the variances and covariance of their binding states:[12]

$$\rho_{ij} = \frac{\mathrm{cov}(n_i, n_j)}{[\mathrm{var}(n_i)\mathrm{var}(n_j)]^{1/2}} \quad (1)$$

where n_i is the occupancy (0 or 1) of site i.

The correlation between two sites is not a constant of the system but rather a function of its thermodynamic state and, in this case, a function of pH and E. However, this is only possible because the constant-(pH,E) MD method considers both redox and protonation equilibria.[12,16,27] From an electrostatic point of view, we expect directly interacting protonable and redox sites to be positively correlated, as protons and electrons tend to stabilize each other. The exact opposite is expected for homotropic interactions, i.e. interactions between redox sites, in this case heme−heme interactions.[12,13,27] However, indirect interactions may result in less obvious coupling events.[12,16,27]

All directly interacting redox sites, i.e., hemes I−II, I−III, and III−IV (see Figure 5a), were found to be negatively correlated throughout the simulated E range. This finding agrees with our electrostatics based reasoning and with previously published studies.[12,13,16,27] However, all of these theoretical results contrast with experimental ones published by Turner et al.[4] These authors showed that hemes I and II exhibit a positive cooperativity that none of the aforementioned studies, including ours, predicts. In fact, our results show that hemes I and II possess a strong negative correlation, meaning that at each simulated E, hemes I and II tend to be in opposite redox states. The indirect interaction of hemes I and II, mediated by propionate D from heme I, does not seem to be strong enough to overcome the destabilizing direct interaction between hemes. This was reported by Baptista et al., and suggested to be a consequence of the lack of conformational rearrangements in the models then used (rigid-structure PB/MC).[12,27] Recently, Machuqueiro and Baptista obtained the same results with the constant-(pH,E) MD methodology, which includes conformational rearrangements explicitly as a consequence of the MD steps.

The direct interactions between protonable and redox sites present at the pH value used in this work are between histidine 67 and hemes II and IV, and between the N-terminal and heme

dx.doi.org/10.1021/jp3082134 | J. Phys. Chem. B 2013, 117, 70−82

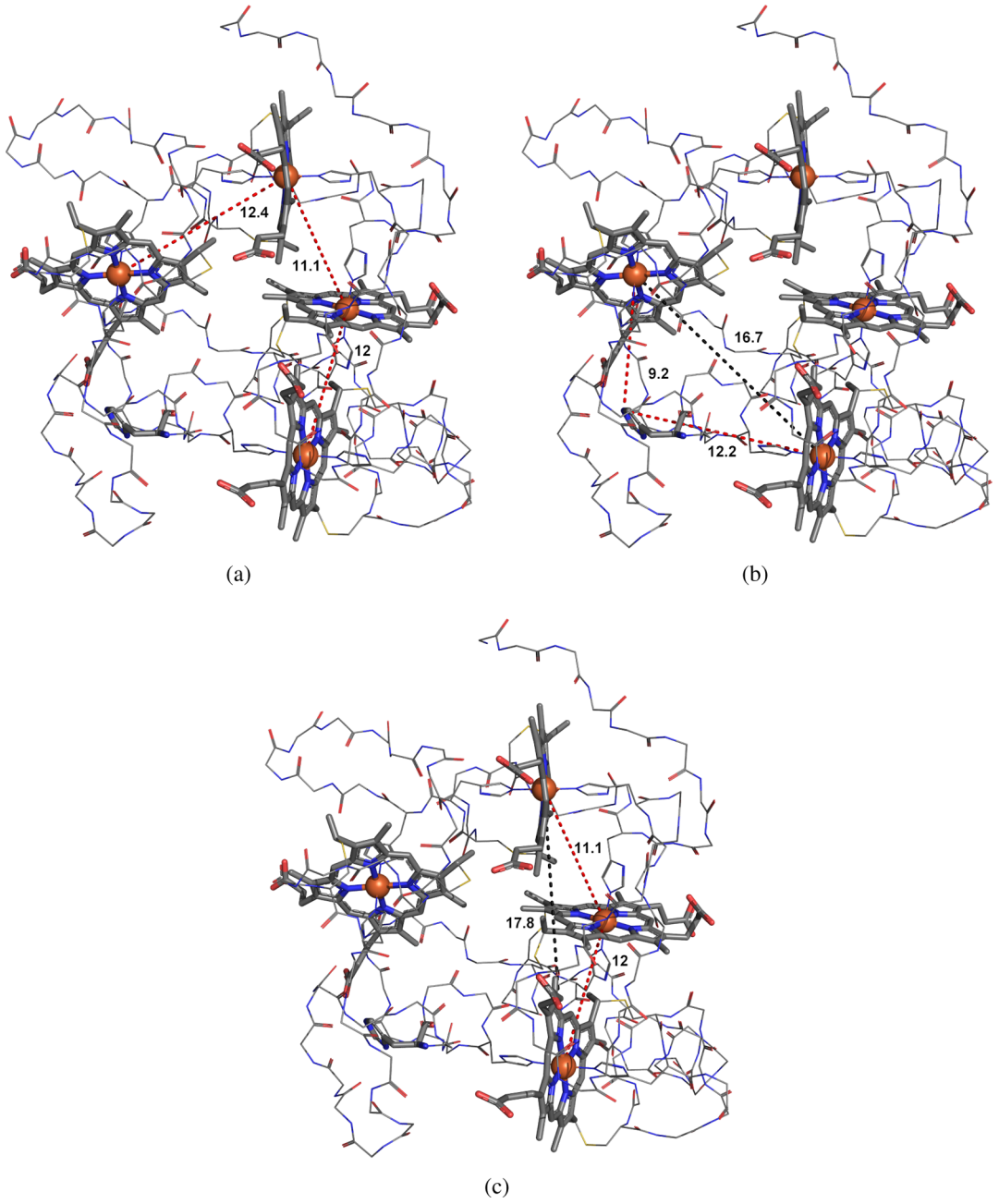

Figure 5. Schematic representation of the most common (in)direct interactions between pairs of sites. (a) Homotropic direct interactions between hemes. (b) Indirect interaction between hemes II and IV, mediated by a simultaneous heterotropic direct interaction with histidine 67. (c) Indirect interaction between hemes I and IV through a simultaneous homotropic direct interaction with heme III. The distances (in Å) between the iron atoms and iron atoms and His67 are presented to illustrate the correlations type.

I. We were unable to obtain any correlations involving the N-terminal above the established cutoff of 0.08, but most simulations produced significant correlations between histidine 67 and hemes II and IV. In general terms, these correlations were positive, meaning that at the simulated pH there are correlated electron and proton titrations in the same molecule, i.e., redox-Bohr effect is in agreement with previous studies.[12,13,16,27] Correlations between hemes I and IV and II and IV result from indirect interactions mediated by other redox/protonable sites (see Figure 5b,c). This type of interaction is very sensitive to changes in charge set and simulated *E* values. From our simulations, we observed several indirect interactions using different conditions. Table 5 presents these examples of unlikely positive cooperativities established by indirect interactions. Correlations of any kind between hemes II and IV were not noticeable in most studies.[12,16,27] Yet, because these two heme groups are positively correlated with the protonable site histidine 67, they are prone to exist in the same redox state. Interactions involving propionates were small probably due to lack of sampling in the propionate titration at the simulated pH. An important result is that the correlations obtained with this work are, in absolute terms, higher than any of those previously published by Baptista et al.[12,16,27] This is most probably due to the fact that the authors used a higher dielectric constant in their studies.

dx.doi.org/10.1021/jp3082134 | *J. Phys. Chem. B* 2013, 117, 70−82

Table 5. Correlations between Pairs of Sites[a]

simulation	E (mV)	interaction	correlation
RESP	−295	II−H67	0.170
		IV−H67	0.230
		II−IV	**0.140**
RESP MC free	−313	I−III	−0.257
		III−IV	−0.123
		I−IV	**0.083**
	−253	II−H67	0.153
		IV−H67	0.082
		II−IV	**0.154**
RESP MC fixed	−291	I−III	−0.249
		III−IV	−0.089
		I−IV	**0.101**
MK	−315	I−III	−0.137
		III−IV	−0.136
		I−IV	**0.208**

[a]Interactions in bold are considered indirect.

As noted before by Baptista et al.,[12] given certain E values it is possible to define overall electronic states for *Dv*H-c_3, according to the individual computed E^{half} values for each heme group. For example, at a reduction potential close to the global midpoint reduction potential, there are on average two heme reducing electrons present in the system. However, only approximately half of the total protein population is composed by molecules with two electrons. In fact, each average reduction, $\langle n_e \rangle$, which goes from 0 (fully oxidized) to 4 (fully reduced), presents wide distributions of the total number of electrons (see Figure 6 and Figure S2). This is explained because under nonequilibrium conditions, *Dv*H-c_3 can act as a reservoir of electrons, accommodating a deficit or excess of electrons. It is considered to be crucial for *Dv*H-c_3 function, enabling it to perform its characteristic concerted transfer of two electrons and two protons, i.e., proton thrusting energy transduction.[2,77]

CONCLUSIONS

The work reported here derives from the new implementation and extension of the stochastic titration method,[27] which makes it possible to perform MD simulations at constant pH and E: the constant-(pH,E) MD method.[16] The previous application of this method to *Dv*H-c_3 only yielded good performances when the protein region was assigned a high dielectric constant. This was unexpected because the method should have allowed the use of $\varepsilon = 2$[27] and called our attention to the possibility of a poor heme group charge parametrization.

In this work, we tested six different charge sets, using three distinct ESP charge derivation approaches (MK, CHELPG and RESP), and concluded that more accurate charge sets greatly improved past results,[16] overcoming the aforementioned dependency on the dielectric constant assigned to the protein. We obtained a clear, method-independent, concerted shift of the computed E^{mod} toward more reasonable values (<−220 mV), while maintaining an accuracy within the error associated with the stochastic titration method.[30] This finding shows the importance of a good quantum description of the system and of constraining the charges from atoms deeply buried within the molecular surface during the fitting procedure.

We were able to predict the exact order of reduction of some heme groups. Hemes I and II were predicted with great precision in most cases but Hemes III and IV midpoint reduction potentials appear to be swapped, being in opposite extremes when compared to experimental data. This is difficult to interpret, especially because of the systematic nature of the results and also because there were no signs of ambiguity in heme group numbering in the original experimental work.[5]

Our simulations reveal a strong coupling between hemes in close proximity, in good agreement with previous work[12,14,16] and experimentally derived data,[4] with the exception of any positive cooperativity between hemes I and II. This absence of cooperative effects may be an important factor preventing our method from achieving better predictive power. We also show that the partially reduced protein can act as an electron buffer, accommodating a number of titrating electrons below or above its average value, which may be relevant under nonequilibrium conditions.

All tested charge sets and respective charge parametrization methods constitute valid approaches, as long as they are derived from accurate QM computations and thoughtful rational. This work does not allow us to select unequivocally one method as the best. Yet, the RESP fitting procedure is much more versatile than CHELPG and MK, making it a better suited tool for generalized derivation of partial atomic charges.

ASSOCIATED CONTENT

Supporting Information

Three tables showing the crossed RMSD between the different charge sets. One figure showing the average variation of each partial atomic charge between charge sets. Histograms of the electron populations at different average reduction for each charge set. This material is available free of charge via the Internet at http://pubs.acs.org.

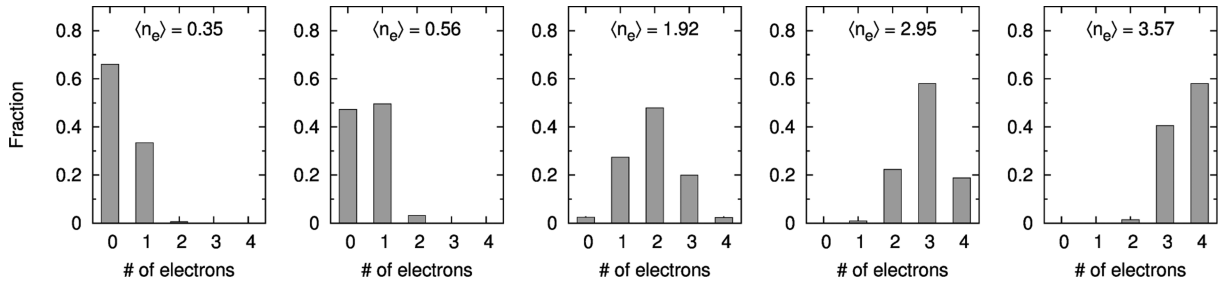

Figure 6. Histograms of the electron populations at different average reduction ($\langle n_e \rangle$) for the RESP charge set. The reduction values range from 0 (fully oxidized) to 4 (fully reduced). From left to right: E = −140, −180, −240, −280, and −320 mV. For the remainder charge sets, see the Supporting Information.

dx.doi.org/10.1021/jp3082134 | J. Phys. Chem. B 2013, 117, 70−82

AUTHOR INFORMATION

Corresponding Author

*E-mail: machuque@fc.ul.pt. Phone: +351-21-7500112. Fax: +351-21-7500088.

Notes

The authors declare no competing financial interest.

ACKNOWLEDGMENTS

We thank António M. Baptista and Diogo Vila Viçosa for fruitful discussions. We acknowledge financial support from Fundação para a Ciência e Tecnologia, through Project PEst-OE/QUI/UI0612/2011 and Grant SFRH/BPD/27082/2006.

REFERENCES

(1) Papa, S.; Guerrieri, F.; Izzo, G. *FEBS Lett.* **1979**, *105*, 213−216.
(2) Louro, R. O.; Catarino, T.; Salgueiro, C. A.; LeGall, J.; Xavier, A. V. *J. Biol. Inorg. Chem.* **1996**, *1*, 34−38.
(3) Turner, D. L.; Salgueiro, C. A.; Catarino, T.; LeGall, J.; Xavier, A. V. *Biochem. Biophys. Acta* **1994**, *1187*, 232−235.
(4) Turner, D. L.; Salgueiro, C. A.; Catarino, T.; LeGall, J.; Xavier, A. V. *Eur. J. Biochem.* **1996**, *241*, 723−731.
(5) Turner, D. L.; Salgueiro, C. A.; LeGall, J.; Xavier, A. V. *Eur. J. Biochem.* **1992**, *210*, 931−936.
(6) Xavier, A. V. *J. Inorg. Biochem.* **1986**, *28*, 239−243.
(7) Johnson, M. K.; Zambrano, I. C.; Czechowski, M. H.; Peck, H. D.; DerVartanian, D. V.; LeGall, J.; Xavier, A. V. In *Frontiers in bioinorganic chemistry*; Xavier, A. V., Ed.; VCH Publishers: Weinheim, Germany, 1985; pp 36−44.
(8) Louro, R. O.; Catarino, T.; LeGall, J.; Turner, D. L.; Xavier, A. V. *ChemBioChem* **2001**, *2*, 831−837.
(9) Bendall, D. S. *Protein Electron Transfer*; Bios Scientific Publishers: Oxford, U.K., 1996.
(10) Soares, C. M.; Martel, P. J.; Carrondo, M. A. *J. Biol. Inorg. Chem.* **1997**, *2*, 714−727.
(11) Soares, C. M.; Martel, P. J.; Mendes, J.; Carrondo, M. A. *Biophys. J.* **1998**, *74*, 1708−1721.
(12) Baptista, A. M.; Martel, P. J.; Soares, C. M. *Biophys. J.* **1999**, *76*, 2978−2998.
(13) Martel, P. J.; Soares, C. M.; Baptista, A. M.; Fuxreiter, M.; Náray-Szabó, G.; Louro, R. O.; Carrondo, M. A. *J. Biol. Inorg. Chem.* **1999**, *4*, 73−86.
(14) Teixeira, V. H.; Soares, C. M.; Baptista, A. M. *J. Biol. Inorg. Chem.* **2002**, *7*, 200−216.
(15) Teixeira, V. H.; Baptista, A. M.; Soares, C. M. *Biophys. J.* **2004**, *86*, 2773−2785.
(16) Machuqueiro, M.; Baptista, A. M. *J. Am. Chem. Soc.* **2009**, *131*, 12586−12594.
(17) Börjesson, U.; Hünenberger, P. H. *J. Chem. Phys.* **2001**, *114*, 9706−9719.
(18) Mertz, J. E.; Pettitt, B. M. *Int. J. High Perform. Comput. Appl.* **1994**, *8*, 47−53.
(19) Börjesson, U.; Hünenberger, P. H. *J. Phys. Chem. B* **2004**, *108*, 13551−13559.
(20) Stern, H. A. *J. Chem. Phys.* **2007**, *126*, 164112.
(21) Walczak, A. M.; Antosiewicz, J. M. *Phys. Rev. E* **2002**, *66*, 051911.
(22) Długosz, M.; Antosiewicz, J. M.; Robertson, A. D. *Phys. Rev. E* **2004**, *69*, 021915.
(23) Długosz, M.; Antosiewicz, J. M. *Chem. Phys.* **2004**, *302*, 161−170.
(24) Mongan, J.; Case, D. A.; McCammon, J. A. *J. Comput. Chem.* **2004**, *25*, 2038−2048.
(25) Khandogin, J.; Brooks, C. L. *Biophys. J.* **2005**, *89*, 141−157.
(26) Khandogin, J.; Brooks, C. L. *Biochemistry* **2006**, *45*, 9363−9373.
(27) Baptista, A. M.; Teixeira, V. H.; Soares, C. M. *J. Chem. Phys.* **2002**, *117*, 4184−4200.
(28) Machuqueiro, M.; Baptista, A. M. *J. Phys. Chem. B* **2006**, *110*, 2927−2933.
(29) Machuqueiro, M.; Baptista, A. M. *Biophys. J.* **2007**, *92*, 1836−1845.
(30) Machuqueiro, M.; Baptista, A. M. *Proteins: Struct. Funct. Bioinf.* **2008**, *72*, 289−298.
(31) Campos, S. R. R.; Baptista, A. M. *J. Phys. Chem. B* **2009**, *113*, 15989−16001.
(32) van Gunsteren, W. F.; Berendsen, H. J. C. *Angew. Chem., Int. Ed.* **1990**, *29*, 992−1023.
(33) Cramer, C. J. *Essentials of computational chemistry: Theories and models*; John Wiley & Sons Inc: West Sussex, England, 2004.
(34) Scott, W. R. P.; Hünenberger, P. H.; Tironi, I. G.; Mark, A. E.; Billeter, S. R.; Fennen, J.; Torda, A. E.; Huber, T.; Krüger, P.; Van Gunsteren, W. F. *J. Phys. Chem. A* **1999**, *103*, 3596−3607.
(35) Oostenbrink, C.; Soares, T. A.; van der Vegt, N. F. A.; van Gunsteren, W. F. *Eur. Biophys. J.* **2005**, *34*, 273−284.
(36) Oliveira, A. S. F.; Teixeira, V. H.; Baptista, A. M.; Soares, C. M. *Biophys. J.* **2005**, *89*, 3919−3930.
(37) Singh, U. C.; Kollman, P. A. *J. Comput. Chem.* **1984**, *5*, 129−145.
(38) Besler, B. H.; Merz, K. M., Jr.; Kollman, P. A. *J. Comput. Chem.* **1990**, *11*, 431−439.
(39) Breneman, C. M.; Wiberg, K. B. *J. Comput. Chem.* **1990**, *11*, 361−373.
(40) Bayly, C. I.; Cieplak, P.; Cornell, W.; Kollman, P. A. *J. Phys. Chem.* **1993**, *97*, 10269−10280.
(41) Sigfridsson, E.; Ryde, U. *J. Comput. Chem.* **1998**, *19*, 377−395.
(42) Martin, F.; Zipse, H. *J. Comput. Chem.* **2005**, *26*, 97−105.
(43) Mulliken, R. S. *J. Chem. Phys.* **1955**, *23*, 1841−1846.
(44) Woods, R. J.; Chappelle, R. *J. Mol. Struct. (THEOCHEM)* **2000**, *527*, 149−156.
(45) Coutinho, I. B.; Xavier, A. V. *Methods Enzymol.* **1994**, *243*, 119−140.
(46) Pereira, I.; Teixeira, M.; Xavier, A. V. *Bioinorg. Chem.* **1998**, 65−89.
(47) Frisch, M. J. et al. *Gaussian 03*; Gaussian, Inc.: Wallingford, CT, 2004.
(48) Becke, A. D. *Phys. Rev. A* **1988**, *38*, 3098−3100.
(49) Lee, C.; Yang, W.; Parr, R. G. *Phys. Rev. B* **1988**, *37*, 785−789.
(50) Vosko, S. H.; Wilk, L.; Nusair, M. *Can. J. Phys* **1980**, *58*, 1200−1211.
(51) Roy, L. E.; Hay, P. J.; Martin, R. L. *J. Chem. Theory Comput.* **2008**, *4*, 1029−1031.
(52) Hariharan, P. C.; Pople, J. A. *Theor. Chem. Acc.* **1973**, *28*, 213−222.
(53) Rassolov, V. A.; Pople, J. A.; Ratner, M. A.; Windus, T. L. *J. Chem. Phys.* **1998**, *109*, 1223−1229.
(54) Francl, M. M.; Pietro, W. J.; Hehre, W. J.; Binkley, J. S.; Gordon, M. S.; DeFrees, D. J.; Pople, J. A. *J. Chem. Phys.* **1982**, *77*, 3654−3665.
(55) Matias, P. M.; Frazão, C.; Morais, J.; Coll, M.; Carrondo, M. A. *Mol. Biol.* **1993**, *234*, 680−699.
(56) Simões, P.; Matias, P. M.; Morais, J.; Wilson, K.; Dauter, Z.; Carrondo, M. A. *Inorg. Chim. Acta* **1998**, *273*, 213−224.
(57) Guha, R.; Howard, M. T.; Hutchison, G. R.; Murray-Rust, P.; Rzepa, H.; Steinbeck, C.; Wegner, J.; Willighagen, E. L. *J. Chem. Inf. Model* **2006**, *46*, 991−998.
(58) Scheidt, W. R.; Reed, C. A. *Chem. Rev.* **1981**, *81*, 543−555.
(59) Gadsby, P. M. A.; Thomson, A. J. *J. Am. Chem. Soc.* **1990**, *112*, 5003−5011.
(60) Ma, J.-G.; Zhang, J.; Franco, R.; Jia, S.-L.; Moura, I.; Moura, J. J. G.; Kroneck, P. M. H.; Shelnutt, J. A. *Biochemistry* **1998**, *37*, 12431−12442.
(61) Case, D. A.; Cheatham, T. E., III; Darden, T.; Gohlke, H.; Luo, R.; Merz, K. M., Jr; Onufriev, A.; Simmerling, C.; Wang, B.; Woods, R. J. *J. Comput. Chem.* **2005**, *26*, 1668−1688.
(62) Dupradeau, F. Y.; Pigache, A.; Zaffran, T.; Savineau, C.; Lelong, R.; Grivel, N.; Lelong, D.; Rosanski, W.; Cieplak, P. *Phys. Chem. Chem. Phys.* **2010**, *12*, 7821−7839.

(63) Bashford, D.; Gerwert, K. *J. Mol. Biol.* **1992**, *224*, 473−486.
(64) Berendsen, H. J. C.; van der Spoel, D.; van Drunen, R. *Comput. Phys. Commun.* **1995**, *91*, 43−56.
(65) Lindahl, E.; Hess, B.; van der Spoel, D. *J. Mol. Model.* **2001**, *7*, 306−317.
(66) Hermans, J.; Berendsen, H. J. C.; van Gunsteren, W. F.; Postma, J. P. M. *Biopolymers* **1984**, *23*, 1513−1518.
(67) Hess, B.; Bekker, H.; Berendsen, H. J. C.; Fraaije, J. G. E. M. *J. Comput. Chem.* **1997**, *18*, 1463−1472.
(68) Tironi, I. G.; Sperb, R.; Smith, P. E.; van Gunsteren, W. F. *J. Chem. Phys.* **1995**, *102*, 5451−5459.
(69) Berendsen, H. J. C.; Postma, J. P. M.; van Gunsteren, W. F.; DiNola, A.; Haak, J. R. *J. Chem. Phys.* **1984**, *81*, 3684−3690.
(70) DeLano, W. L. *The PyMOL User's Manual*; DeLano Scientific: San Carlos, CA, 2002.
(71) Zhurko, G. A.; Zhurko, D. A. Chemcraft: Graphical program for working with quantum chemistry computations, version 1.6. 2009.
(72) Crawford, D. Gnuplot: An interactive plotting program, version 4.2. 2007.
(73) Allen, P. M.; Tildesley, D. J. *Computer Simulation of Liquids*; Clarendon: Oxford, U.K., 1997.
(74) Paquete, C. M.; Turner, D. L.; Louro, R. O.; Xavier, A. V.; Catarino, T. *Biochem. Biophys. Acta* **2007**, *1767*, 1169−1179.
(75) Harbury, H. A.; Cronin, J. R.; Fanger, M. W.; Hettinger, T. P.; Murphy, A. J.; Myer, Y. P.; Vinogradov, S. N. *Proc. Natl. Acad. Sci. U.S.A.* **1965**, *54*, 1658.
(76) Oostenbrink, C.; Villa, A.; Mark, A. E.; van Gunsteren, W. F. *J. Comput. Chem.* **2004**, *25*, 1656−1676.
(77) Louro, R. O.; Catarino, T.; LeGall, J.; Xavier, A. V. *J. Biol. Inorg. Chem.* **1997**, *2*, 488−491.